THE ASTRONOMICAL JOURNAL, 119:111–118, 2000 January

STUDY OF McLEISH'S INTERACTING OBJECT

R. DÍAZ,[1,2] I. RODRIGUES,[3,4] H. DOTTORI,[3] AND G. CARRANZA[1,5]

Received 1999 June 15; accepted 1999 September 21

ABSTRACT

We discuss the morphology, kinematics, and physical conditions of the emitting gas of the interacting system IRAS 20048−6621. We present as well numerical simulations of this interacting system, discovered by David McLeish in 1946. The main galaxy (McL A) is an edge-on spiral galaxy with highly distorted NW side. On this side is also located McL B, the perturber galaxy. We determined a distance of 151 Mpc ($h = 0.75$) and a diameter of 70 kpc for McL A. It presents a bright nucleus with broad red emission lines ($\langle \mathrm{FWHM} \rangle \approx 500$ km s^{-1}). McL A has far-IR color indexes closely comparable to NGC 3628, one the few nearby edge-on galaxies which is a bright infrared emitter. Nevertheless, McL A is more luminous (in these bands) than any of the edge-on galaxies in the sample of bright infrared galaxies of Young et al. (1988). The two sides of McL A rotation curve are remarkably different. The N-body model that best reproduces McL A kinematical and morphological data (Kuijken & Dubinski 1995) gives a total mass 7×10^{11} $M_{\odot}$ for McL A. Numerical simulations with the TREESPH code closely reproduce the morphology and radial velocity observations. The best scenario for this system is that of a prograde encounter between McL A and B, with McL B's orbit 35° tilted with respect to the spiral disk of McL A and a perigalactic distance of 17.6 kpc. The derived mass ratio is McL B/McL A ≈ 1/26. In the last 5×10^8 yr the perturber has crossed the main galaxy disk twice, in between it crossed the perigalacticon. According to our simulations, the emitting gas present in McL B has not been stripped out from the McL A disk, so that leads us to conclude that McL B is an irregular or small spiral galaxy.

Key words: galaxies: binary — galaxies: individual (McLeish's object) — galaxies: interactions — galaxies: kinematics and dynamics — galaxies: nuclei — galaxies: peculiar

1. INTRODUCTION

McLeish's object (AM 2004−662, IRAS 20048−6621; $\alpha(\mathrm{J2000}) = 20^{\mathrm{h}}09^{\mathrm{m}}28\overset{\mathrm{s}}{.}1$, $\delta = -66°13'00''$, near the bright star δ Pavonis, was discovered in 1946 by the astronomer David McLeish, of Córdoba Observatory. Sérsic (1968), based on 30 minute exposure 103aO plates, described the object as very long and narrow, with a bend at the southern end. He also suggested that it could be an intergalactic "shred," in the Arp (1967) sense, although this type of structure always appears associated with a large galaxy. Arp, Madore, & Robertson (1987) briefly describe the main galaxy as elongated, with an interacting companion, question marking "shred?" A very similar system is AM 0302−504, which seems to represent an encounter in the same evolutionary stage, but seen from a different angle.

Other observations of this object have been made by Johansson & Bergvall (1990), who carried out broadband photoelectric photometry, and by Allen et al. (1991), who determined its radial velocity, both of them as part of large surveys. Our interest in this object was renewed, because it was detected by *IRAS* as the point source IRAS 20048−6621. We performed CCD imaging and spectroscopy with the 1.54 m reflector telescope of Córdoba Observatory. The first images revealed the presence of a companion and intergalactic debris, which strongly suggested a couple of galaxies in interaction. The full set of observations were complemented with numerical N-body/SPH (TREESPH; Hernquist & Katz 1989) simulations in order to reproduce the dynamical history that yielded the present configuration of the McLeish perturbed system. From the simulation point of view this is important, since it is a rare case of a strictly edge-on interacting galaxy. It is important to point out that TREESPH has already been successfully applied by our group to reproduce interchange of matter between a globular cluster and the bulge environment of the Milky Way (Bica et al. 1997) and to discuss the interacting system NGC 6845 (Rodrigues et al. 2000).

In § 2 we present the observations and in § 3 the results, which are discussed in § 4.

2. OBSERVATIONS AND DATA REDUCTION

The observations have been performed at the 1.54 m telescope of Bosque Alegre Astrophysical Station, using the instrument MIFiS (for a brief description see Díaz et al. 1999). The operation of the telescope, MIFiS, and control computers were performed in accordance with the procedures detailed by Díaz et al. (1997).

The data were gathered in several observing runs dedicated to an extragalactic observation program during 1997 and 1998.

In the long-slit mode we used a 1200 grooves mm^{-1} grating in first order, giving a dispersion of 0.78 Å pixel^{-1}. The slit width was 2″, yielding a resolution of ≈3 Å. We obtained about 8 hr of spectra in three different position angles (P.A.), all of them through the nucleus. Zero-order imaging allowed us to register the slit positions with high precision. We also performed 3 hr of low-resolution spectra (≈12 Å) with a 300 grooves mm^{-1} grating in first order. During the observations seeing was $1''.8 \leq \mathrm{FWHM} \leq 2''.8$.

We also obtained direct images in the Johnson photometric bands B, V, R, and I, totaling 20 minutes of exposure

[1] Observatorio Astronómico de Córdoba, UNC, Laprida 854, 5000 Córdoba, Argentina.
[2] FoMEC, Facultad de Matemática, Astronomía y Física, UNC, Argentina.
[3] Instituto de Física, UFRGS, CP 15051, Av. B. Gonçalves 9500, Porto Alegre, Brazil.
[4] CNPq fellow.
[5] CONICET, Argentina.

in each band. These images were calibrated with the nearby bright star δ Pavonis.

The reduction was accomplished mainly with ADHOC reduction software (Marseille Observatory; Boulesteix 1993), and standard techniques for two-dimensional detectors were applied for the reduction of images and spectral frames. Spectra extractions were performed in slices of 3″ in the central portions of the frames and 6″ in the regions with lower S/N ratio. After wavelength calibration, the instrumental width of the night-sky emission lines was $\approx$140 km s^{-1} and the spectra were corrected with the mean transmission function of the observing system, obtained from Stone & Baldwin's (1983) spectrophotometric standards.

The emission line parameters were interactively fitted with Gaussian profiles. In the regions of S/N $\geq$ 10 (central 10″), we fitted Gaussians to the lines Hα λ6563, [N II] λ6548, 6584 and [S II] λ6717, 6731. In the regions of lower S/N we only fitted the Hα emission line.

2.1. *Kinematics Reduction*

Radial velocities have been determined along $\approx$90″ ($\approx$66 kpc, Fig. 6*c*). We used the formula

$$V_r = c = c[(1 + z)^2 - 1]/[(1 + z^2) + 1] ,$$

where $z = \delta\lambda/\lambda$.

Since most of the radial velocities were measured from one emission line, we used Keel's expression (Keel 1996b) for the determination of the uncertainty of each velocity value, both for line barycenter and for Gaussian peak determination:

$$e_{\rm bar} = (\sigma_{\rm con}/I_{\rm H\alpha})(\delta\lambda^{1.5}/\lambda)(c/d^{0.5})$$

(error propagation),

$$e_{\rm gau} = 0.8(\sigma_{\rm con}/I_{\rm H\alpha})(\delta\lambda^{1.5}/\lambda)(c/d^{0.5}) \quad (1)$$

(empirical), where $\sigma_{\rm con}$ is the noise at continuum level and $I_{\rm H\alpha}$ is the line intensity, both in ADU; $\delta\lambda$ is the lines FWHM and d is the dispersion of the spectrum, in angstroms per pixel.

In the nuclear region, where we had several lines to check independently the radial velocity error, the value was close to that derived from equation (1), so we found it reasonable to adopt the uncertainty values given by equation (1) for all the Hα radial velocity determinations. This uncertainty is 15 km s^{-1} for the nucleus, increasing up to $\approx$100 km s^{-1} at the external portion of the radial velocity curve.

3. RESULTS

3.1. *Morphology and Photometry*

3.1.1. *Optical Data*

McL A (Fig. 1) has an elongated appearance, and at the unperturbed extreme (SE) it has an integrated major-axis profile typical of an edge-on spiral galaxy; when compared with the radial brightness profiles of Boroson (1981), it is between those of NGC 1058 (Sc) and NGC 2268 (Sb). McL

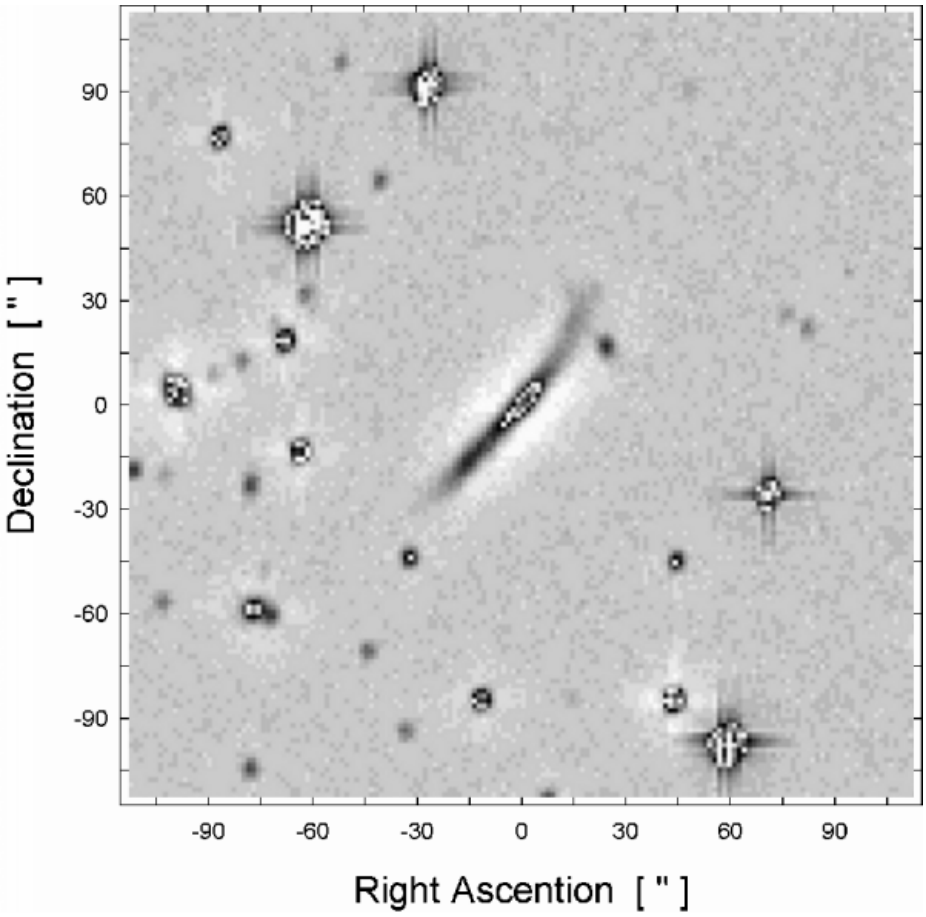

FIG. 1.—*V*-band image of McLeish's object. Total exposure time is 20 minutes.

B is located at 23″ to the NNW of the nucleus of McL A and 7″.5 over the major-axis line, which presents FWHM slightly larger than the seeing. According to the results in § 3.2, the object scale is 1″ = 725 pc ($h = 0.75$).

R-band isophotes show diffuse debris that seems to be connected to McL B and extend for ≈10 kpc, crossing to the opposite side of McL A disk, at an angle of ≈70°.

McL A has an angular major-axis of 94″ (≈69 kpc) at $m_R \approx 24$ mg arcsec^{-2} and P.A. = 139° ± 2°, and the outer radius of the unperturbed side is ≈50″. Its axial ratio is $b/a = 0.15 \pm 0.05$, so we will take it as an edge-on object, what is usually assumed when $b/a \leq 0.3$.

The *B*-band luminosities are -20.5 ± 0.1 mag and -17.8 ± 0.3 mag for McL A and McL B, respectively. McL A's luminosity is typical of the brightest Sb galaxies (Sérsic 1982), and the exponential scale length of the disk is 11 ± 1 kpc, among the largest spiral galaxies (mainly Sb and Sc galaxies). Although the presence of a bright central component is evident in the radial light profiles, the object scale does not allow us to accurately determine the bulge effective radius and the contribution of the bright nucleus to the total luminosity.

The boxy appearance of the McL A disk SE edge is a seeing artifact. We were able to reproduce this effect by Gaussian filtering the images of several nearby edge-on spiral galaxies (NGC 522, NGC 684, NGC 891, NGC 1247, NGC 4452, UGC 711, UGC 1281) in order to match the scale and seeing of Figure 4*a*. (The results also indicate that the morphological type of McL A is possibly Sb or Sc.)

3.1.2. *Far-Infrared Data*

McL A + B is the IR source IRAS 20048−6621 (*IRAS* Point Source Catalog, Version 2). Its far-IR flux density can be calculated as given by Lonsdale et al. (1985):

$$F_{\rm FIR} = (1330 F_{60\mu} + 515 F_{100\mu}) = 2.95(\pm 0.30) \times 10^3 \text{ ergs s}^{-1} \text{ cm}^{-2} .$$

Following Allen et al. (1991), we can calculate the far-IR luminosity:

$$L_{\rm FIR} = \{4 F_{\rm FIR}[1 + z - (1+z)^{1/2}]^2 (1+z)\} \times 10^{10}\ L_\odot ,$$

$$L_{\rm FIR} = 4.5 \times 10^{10}\ h^{-2}\ L_\odot ,$$

where $F_{\rm FIR}$ is in erg s^{-1} cm^{-2}.

53% of the *IRAS* galaxies (e.g., Soifer et al. 1987) emit less IR radiation than McL A + B. The FIR color indexes are $\alpha_{100-60} = -1.67$ and $\alpha_{60-25} = -2.93$. These colors are between those for normal starburst galaxies and those for objects with pure power-law spectral distribution ($F_\nu \propto \nu^\alpha$), according to the criteria of de Grijp, Miley, & Lub (1987).

It is worth noting that from the 15 edge-on galaxies ($i \geq 80°$) in the sample of 192 nearby IR bright galaxies of Young et al. (1989, $\delta > -20°$, $B_T < 12$, $S_{100} > 10$ mJy), only NGC 3079 has FIR luminosity comparable ($1.81 \times 10^{10}\ h^{-2}\ L_\odot$) to that of McL A + B. Moreover, there is only one edge-on galaxy in this sample with FIR color indexes similar to those of McLeish's object. It is NGC 3628, an interacting edge-on spiral galaxy in a compact group (including the bright spirals NGC 3623, NGC 3627, and NGC 3593, at 11 Mpc within the Leo Spur; Tully 1988) that has strong and complex dust lanes. This fact, and the absence of Hβ emission in the low-resolution spectra of McL A nucleus, strongly suggests that this nucleus might be obscured by the disk dust.

3.2. *Spectroscopy*

3.2.1. *McL A Nuclear Physical Conditions*

The nuclear spectra shown in Figure 2, reveal Hα λ6563, [N II] λ6548, 6584 and [S II] λ6717, 6731 emission lines, with a main component $\langle \text{FWHM} \rangle = 520 \pm 40$ km s^{-1} and $\langle V \rangle = 11{,}150 \pm 20$ km s^{-1}, blueshifted with respect to the systemic velocity (see next paragraph). The Hα nuclear emission line shows also a narrow component with $\langle \text{FWHM} \rangle = 350 \pm 40$ km s^{-1}, $\langle V \rangle = 11{,}290 \pm 20$ km s^{-1} and 25% of the flux of the broad component. The observed line ratios are

$$0.74 \leq \text{H}\alpha/[\text{N II}]\lambda 6584 \leq 1.35 ,$$

$$0.80 \leq [\text{S II}](\lambda 6716 + 6731)/\text{H}\alpha \leq 1.10 ,$$

$$0.70 \leq [\text{S II}]\lambda 6716/[\text{S II}]\lambda 6731 \leq 0.80 .$$

The last quotient would indicate $N_e \approx 4000$ cm^{-3}, assuming $T \approx 10{,}000$ K. The two first line ratios are located in the region of the LINER or Seyfert 2 nuclei, in the diagnostics diagrams of Veilleux & Osterbrock (1987). It is not possible to give a definite conclusion because (1) The forbidden lines, especially [N II] λ6584, are strongly contaminated by the OH[7–2] ($\lambda\lambda$6863.94–7082.2; Osterbrock & Martel 1994) night-sky lines, so sky subtraction becomes difficult; (2) the low-dispersion spectra ($\lambda\lambda$4400–7600 Å) shows no traces of Hβ and [O III] λ5007 emission lines at 2 σ level, possibly due to the dust absorption (§ 3.1), which restricts the use of the diagnostic diagrams.

3.2.2. *Kinematics*

The rotation curve (see Fig. 6*c*) seems to be of the solid-body kind in more than 80% of McL A's diameter. We took the continuum spectra nuclear barycenter as origin of the radial distances. We then adopted as heliocentric systemic velocity the mean value of the linear part of the rotation curve, from $r = -20''$ to $r = +20''$. We obtained a value of $V_{\rm sys} = 11300 \pm 30$ km s^{-1}, consistent with the value given by Allen et al. (1991) in the Anglo-Australian Telescope radial velocity survey. This value is also in agreement with the radial velocity of the narrow component in the nuclear emission lines (previous paragraph).

Considering the local motion of 300 km s^{-1} toward $l = 90°$, $b = 0°$ we obtain $V_0 = 11{,}200 \pm 30$ km s^{-1} and a distance of 149 ± 1 Mpc ($h = 0.75$).

At the disk extremes, the rotation curve departs from the linear trend in different ways, which might indicate the influence of the interaction with McL B. The amplitude of the rotation curve is significantly larger on the unperturbed side (SE), amounting to 400 ± 100 km s^{-1}, whereas the maximum radial velocity difference between both extremes

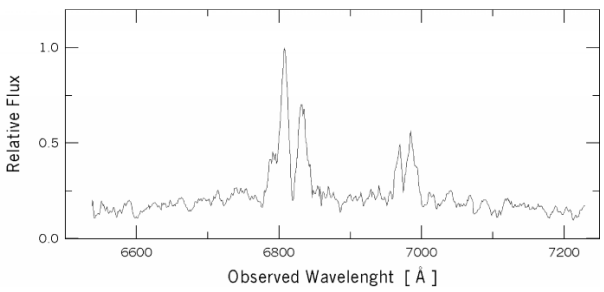

FIG. 2.—Central 3″ spectrum. Total exposure time is 4 hr.

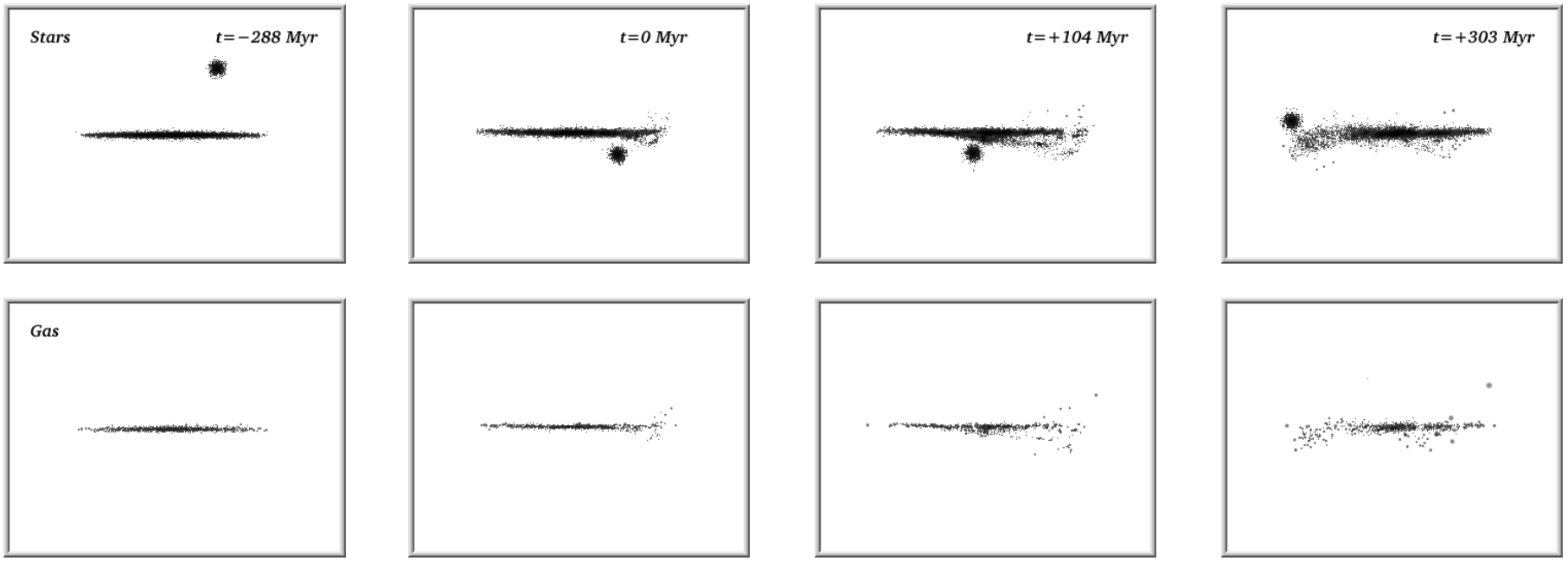

FIG. 3.—Four selected steps of the time evolution of the final model, run 10. The top row shows the stellar content, while the bottom row shows the gas particles. The frames side measure 154 kpc. Run time with respect to the perigalacticon is shown at the upper right.

is 600 ± 120 km s^{-1}. A Satoh (1980) model fit as well as simple Keplerian model both lead to a mass of $7.0 \pm 0.2 \times 10^{11} M_{\odot}$.

McL B shows a weak Hα emission line, which only gives a recession velocity of $11{,}500 \pm 100$ km s^{-1}, quite similar to that of McL A.

3.3. *Encounter Modeling*

The morphology and velocity field of McL A + B system strongly suggest that these galaxies are suffering a close encounter. In order to study the dynamical history of this system we simulated the encounter, following the evolution of the stellar and gaseous content of the galaxies.

The simulations were run in a Cray T94 computer (CESUP-UFRGS) and evolved in time using the TREESPH code (Hernquist & Katz 1989). The code particle-shell force calculations were performed with opening angle $\theta \leq 0.7$ and quadrupole cell-mass approximation. Gravity was softened using a spline kernel with a variable softening parameter that includes the 64 nearest neighbors. The force calculation and integration time step were chosen such that the total energy and angular momentum were constant to within 0.02% and 0.1%, respectively, over the course of each simulation. The simulations start with both galaxy models separated by a distance of 88 kpc.

McL A model (Figs. 3*a* and 5*a*) was constructed as a self consistent disk-bulge-halo galaxy model, following the general prescription of Kuijken & Dubinsky (1995). This method generates near-equilibrium phase-space distributions of isolated galaxies. The model was done by constraining the amplitude of the rotation curve with the observed one. We obtained a disk + bulge:halo mass ratio of 1:3. In our system of units ($G = 1$) the disk mass is $M_d = 3.36$, its central velocity dispersion is $\sigma_{r,0} = 0.47$ and the disk radial extent (radius where density drops to zero) is $R_t = 11.0$. The small bulge has $M_b = 0.014$ and a radial extent of $R_t = 0.56$, and the halo has $M_h = 9.54$ and radial extent of $R_t = 21.33$. The gas comprises 10% of the disk mass and follows the same density profile as the stellar disk. An isothermal equation of state is chosen for the gas, with temperature $T_{\rm gas} = 10^4$ K. The model units are length, 4 kpc; velocity, 220 km s^{-1}; mass, $5.4 \times 10^{10} M_{\odot}$; and time, 17.296 Myr.

Four different values, between 1/7 and 1/26, were tested for McL B/McL A mass ratio. A few simulations allow us to conclude that the disk of the McL A model is too strongly disturbed by high McL B total mass values. In order to spare computing time, McL B was first represented by a point mass and McL A with 8191 particles. For the best of these simulations (McL B mass equal to 1/26 of McL A mass), the point mass representing McL B was replaced by a lowered Evans distribution (Kuijken & Dubinski 1995), and the particle numbers were raised to 31768 and 1000 for McL A and McL B, respectively.

Table 1 shows the series of simulation runs in which we tested a set of collision parameters. For ease of comparison between simulations and observations we used a coordinate system in which the z-axis corresponds to the line of sight (positive values toward the observer), the xy-plane corresponds to the sky plane, with the x-axis in the direction of the major axis of McL A (positive values to the SE) and the y-axis pointing to the SW. This is the coordinate system used in columns (3) and (4) of Table 1, which indicates the pericenter direction and the orbital spin vector, respectively. The orbital plane is characterized by the orbital spin vector, whose orientation indicates the sense of rotation of the orbit. We used parabolic orbits in all experiments, since as the galaxies fall in toward each other for the first time, they move on simple parabolic orbits.

4. DISCUSSION AND CONCLUDING REMARKS

The most striking feature of this distant system is what seems to be a strong warping of the NW side of the large edge-on disk of McL A galaxy. Furthermore, the deep R-band CCD imagery, revealed the presence of McL B as a small condensation near McL A's disturbed disk end, already noted by Arp et al. (1987), but not detected in the old 103aO plates taken at Córdoba in 1946. The spectroscopy has shown that the radial velocity of McL B galaxy is very close to that of McL A, and the radial velocity curve of McL A has a turnover near the projected position of McL B. These facts suggest then that we are in the presence of an interacting system, where the disturbance of McL A disk is closely related to the presence of McL B, which would be a smaller perturber galaxy.

The presence of a 150 km s^{-1} blueshifted nuclear emission line broad (500 km s^{-1}) component, together with the line ratios Hα/[N II] λ6584, [S II] (λ6716 + 6731)/Hα, as well as the IR colors, point to possible Sy2 like activity in the nucleus of McL A galaxy. This scenario is in good agreement with the study of Keel (1996a), who established that nuclear activity is more frequent in the more luminous members of interacting pairs than in field galaxies. Indeed, the simulations show that the interaction time has been long enough to allow a significant increase of gas density in the central region of McL A, as can be seen when the McL A model initial particle distribution (Fig. 5*a*) is compared to the perturbed one (Fig. 5*b*).

As shown in § 3.2, the amplitude of the rotation curve is large. There are only two disk galaxies in Keel's (1996a) sample of interacting galaxies that present similar (Mrk 1040, $\approx$500 km s^{-1}) or larger (NGC 1144, $\approx$900 km s^{-1}) amplitude of their rotation curve. The rotation curve of Mrk 1040 is of solid body type, as is McL A. Although there are plenty of linear rotation curves among spiral disks (see Mathewson & Ford 1996), it is quite unusual to find a high-luminosity-spiral showing this behavior in more than 80% of its disk diameter. Obviously, this type of rotation curve must appear from perturbations or, more probably, strong content of dust, or both reasons simultaneously. In fact, the luminosity profiles of disk galaxies never point to constant mass density inside these objects. A simple calculation shows that for an optically thick edge-on disk of radius R, the shape of the observed radial velocity curve would be $V_r = [V_c(R)/R]r$, i.e., the rotation curve would appear to grow linearly in this extreme case.

Finally, the sense of rotation of McL A together with McL B relative radial velocity (190 ± 100 km s^{-1}) are compatible with a prograde encounter. It has been clear at least since the Toomre & Toomre (1972) modeling that prograde encounters are most effective in restructuring galaxy disks (see also Negroponte & White 1983; Howard et al. 1993). Although it is an important parameter of an interaction simulation, in order to totally characterize this, we have to know the perigalacticon vector position, as well as McL B's orbital ellipticity and inclination. McL A disk's peculiar position, which is seen practically edge-on, makes it less difficult to obtain a scenario for the collision.

TABLE 1

SIMULATIONS LOG

Run Number (1)	q (2)	$\boldsymbol{q}$ Direction (3)	$\boldsymbol{s}$ Direction (4)	N_A (5)	M_B (6)	N_B (7)
1.....	3.50	(−1, 0, 0)	(0, −1, −1)	8191	0.48	1
2.....	3.50	(−1, 0, 0)	(0, −1, −2.97)	8191	0.48	1
3.....	6.66	(−1, 0, 1)	(−1, −1, −1)	8191	0.48	1
4.....	4.44	(−1, 1, −1)	(−1, −2, −1)	8191	0.48	1
5.....	4.00	(−1, 0, 1)	(−1, −1, −1)	8191	0.88	1
6.....	6.66	(1, 0, 1)	(−1, −3.33, 1)	8191	0.80	1
7.....	6.66	(−1, 0, 1)	(−1, −1, −1)	8191	0.48	1
8.....	4.44	(1, −1, 1)	(−1, −2, −1)	8191	0.48	1
9.....	4.44	(1, −1, 1)	(−1, −2, −1)	31768	1.85	1000
10	4.44	(1, −1, 1)	(−1, −2, −1)	31768	0.48	1000

NOTES.—(Col. [1]) Run number; (col. [2]) pericenter distance q; (col. [3]) pericenter orientation; (col. [4]) orbital spin orientation; (col. [5]) number of particles of McL A model N_A; (col. [6]) mass of McL B model M_B; and (col. [7]) number of particles of McL B model N_B. Data are presented in model units. The model units are length, 4 kpc; velocity, 220 km s^{-1}; and mass, $5.4 \times 10^{10}\ M_\odot$.

The position of McL B is very tricky, because it suggests that the presently observed McL A disk distortion results from a single disk crossing. The first six models of Table 1 were run under this condition, supposing that the present observed configuration is near the perigalacticon. We failed to reproduce the observed McL A disk warping simultaneously with the present galaxy pair configuration. Finally, we decided to change the pericenter direction and orbit inclination in such a way as to have two disk crossings, practically synchronous with a perturbed disk half rotation. The evolution of the best simulation can be seen in Figure 3, corresponding to run number 10 in Table 1. The two galaxies' relative position as well as the perturbed disk warping are in satisfactory agreement with the observed features. Furthermore, a face-on view of the final configuration of the model (Fig. 4; 303 Myr after the perigalacticon) shows that the disk late stage harbors a small tidal tail located at the place of the warping. This view also shows that the McL A model nucleus is displaced from the disk center toward McL B, which explains why the disk's less perturbed side looks longer than the perturbed one in Figure 1 (also in Fig. 6*a*). The model relative radial velocity of McL B at this stage is $\sim$150 km s^{-1}, compatible with the observed value.

The notion of that we see the effects of multiple disk-plane crossings at once has been used as well in studies of M51 (Howard & Byrd 1990; Byrd & Salo 1994). If this proves to be a general phenomenon, modeling galaxies interactions well may involve even more free parameters than previously supposed.

In Figure 5*a* McL A's model initial rotation curve is compared to the perturbed one (Fig. 5*b*) at the model final stage (Fig. 3*d*), 303 Myr after perigalacticon. In order to mimic dust absorption we only consider the near half of the disk. The difference between the approaching and receding (more perturbed) disk edges is dramatic, as the reader may judge for himself. In fact, after the encounter, the approaching side is clearly more populated than the receding one. Also, the rotation curve is wider and more homogenous in the unperturbed side. The central region presents a velocity

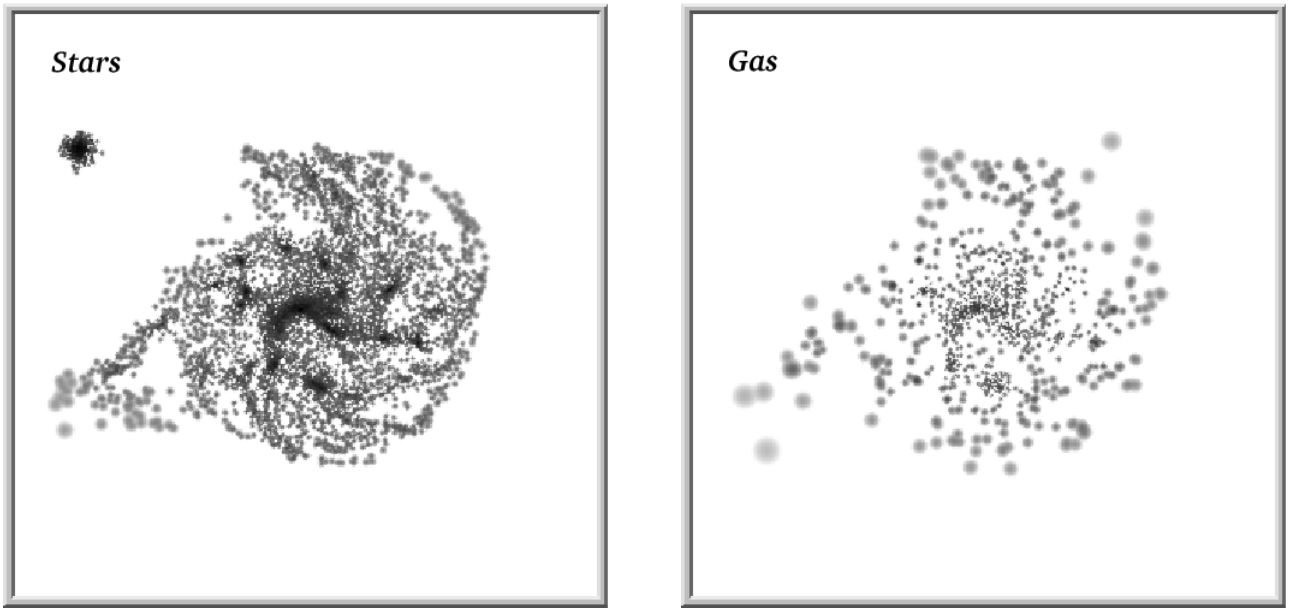

FIG. 4.—Face-on view of the of McL A disk model corresponding to the last frame of Fig. 3 (run 10), 303 Myr after the perigalacticon. For gas particles the representative dots are larger in less dense regions.

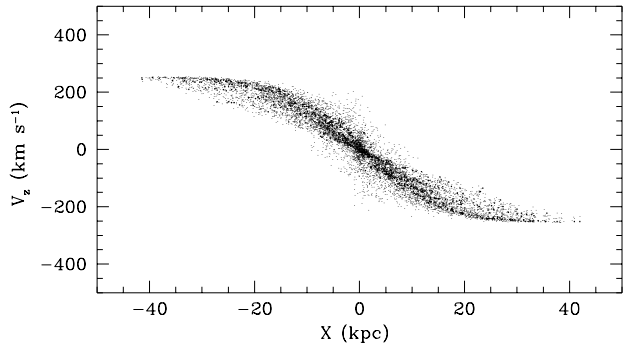

FIG. 5*a*

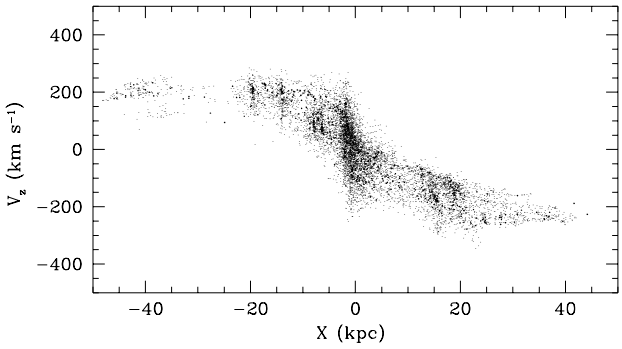

FIG. 5*b*

FIG. 5.—Radial velocity curves of McL A model. Only particles of the nearest half of the disk are shown. Small and large dots represent stellar and gas particles, respectively. (*a*) Isolated model before the interaction. (*b*) Final configuration, corresponding to the last frame of Fig. 3 (run 10), 303 Myr after the perigalacticon. Remarkable kinematic differences arise after the interaction.

dispersion comparable to that observed in the nuclear emission lines Figure 2 and also appears to be blueshifted.

Byrd & Klaric (1990) studied the system AM 2208−251, composed by a roughly edge-on spiral and a smaller round compact E perturber. They inferred the perturber mass from the collision consequences, as we did. Most important from this simulation is that the interaction model produces asymmetry of the rotation curve of the spiral's disk and shows how observations may be misleading in disturbed spirals when one traces rotation curves from H II regions. Although McL B is relatively much less massive with respect to McL A, than the perturber of the mentioned system, it produces also strong kinematical perturbations because in our case the encounter is much more closed.

In Figure 6 we show a direct comparison of the observed galaxy (Fig. 6*a*) and its rotation curve (Fig. 6*c*), with the last step of the Figure 3 run, for which we present stars together with gas particles (Fig. 6*b*). The model rotation curve (Fig. 6*d*) is presented for the outermost ($z \geq 15$ kpc) part of the disk near side, in order to mimic a stronger dust effect than in the previous paragraph in the simulation rotation curve. As can be seen, the solid body rotation curve appearance in

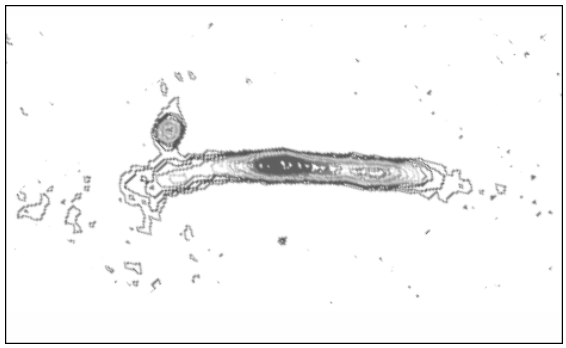

FIG. 6*a*

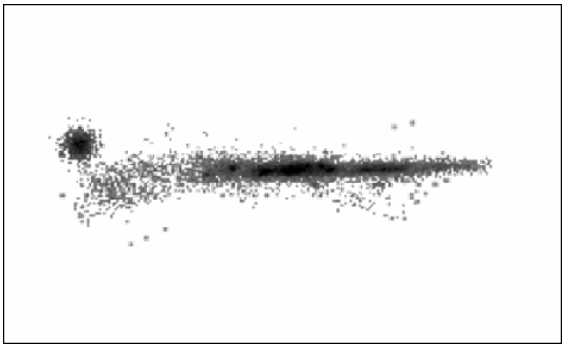

FIG. 6*b*

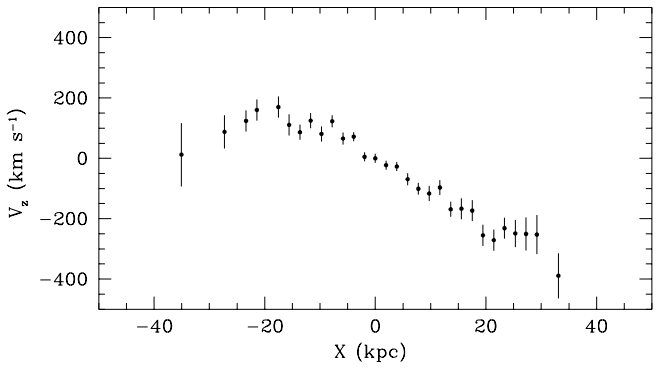

FIG. 6*c*

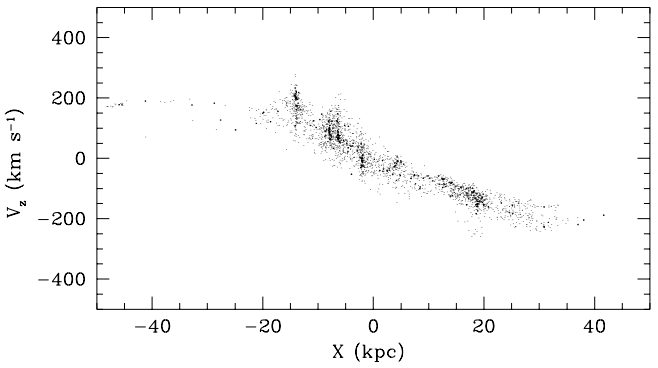

FIG. 6*d*

FIG. 6.—Comparison between McL A's observed morphology and rotation curve, with the model results 303 Myr after the perigalacticon. (*a*) *R*-band image. Total exposure time is 20 minutes. (*b*) Distribution of stars + gas model particles. (*c*) Observed relative radial velocity curve. (*d*) Radial velocity plot for the stellar (*small dots*) and gas (*larger dots*) model particles. Only the near side disk particles' kinematics are presented, from 15 kpc in the *z*-direction, in order to mimic the obscuration effect by dust.

the central 40 kpc or more, is strikingly similar to the observed one. Most of the model rotation curve features discussed in the previous paragraph are present in Figure 6*d*, although they are less obvious because of the smaller number of points.

With regard to McL B we have to mention that it does not strip gas out of the McL A disk under our simulation conditions. This fact leads to the conclusion that this galaxy is of Magellanic type or a small spiral galaxy. The mass derived form the simulation is $\sim 2 \times 10^{10} M_{\odot}$.

Object McLeish has been characterized, both by extensive observations and by successful numerical modeling, as an interacting pair composed of a giant spiral galaxy and a smaller companion.

This work was partially supported by CNPq of Brazil, CONICET and CONICOR of Argentina, and the binational program FAPERGS(98/0967-9)/ ANPCyT(E98U03). R. D. acknowledges the hospitality of the IF-UFRGS (especially to the graduate students friendship) and partial support from Latin American Network of Astronomy supported by UNESCO (COSTED/IBN). Thanks are due to S. Lípari, G. Gimeno, and the staff of Bosque Alegre Astrophysical Station.

REFERENCES

Allen, D., Norris, R., Meadows, V., & Roche, P. 1991, MNRAS, 248, 528
Arp, H. C. 1967, ApJ, 148, 321
Arp, H. C., Madore, B. F., & Roberton, W. E. 1987, A Catalogue of Southern Peculiar Galaxies and Associations, vol. 1 (Cambridge: Cambridge Univ. Press)
Bica, E., Dottori, H., Rodrigues, I., Ortolani, S., & Barbui, B. 1997, ApJ, 482, L49
Boroson, T. 1981, ApJS, 46, 177
Boulesteix, J. 1993, ADHOC Ref. Manual (Marseille: Pub. del'Obs. de Marseille)
Byrd, G., & Klaric, M. 1990, AJ, 99, 1461
Byrd, G., & Salo, H. 1994, BAAS, 26, 917
De Grijp, M., Miley, G., & Lub, J. 1987, A&AS, 70, 95
Díaz, R., Paolantonio, S., Goldes, & G., Carranza, G. 1997, Espectrógrafo Multifunción: Características, Puesta a Punto, Operación y Reducción de Datos, Trabajos de Astronomía Ser. A (Córdoba: National Univ. Córdoba)
Díaz, R., Carranza, G., Dottori, H., & Goldes, G. 1999, ApJ, 512, 623
Hernquist, L., & Katz, N. 1989, ApJS, 70, 419
Howard, S., & Byrd, G. 1990, AJ, 99, 1798
Howard, S., Keel, W., Byrd, G., & Burkey, J. 1993, ApJ, 417, 502
Johansson, L., & Bergvall, N. 1990, A&AS, 86, 167
Keel, W. 1996a, AJ, 111, 696
———. 1996b, ApJS, 106, 27
Kuijken, K., & Dubinski, J. 1995, MNRAS, 277, 1341
Lonsdale, C., Helou, G., Good, J., & Rice, W. 1985, Cataloged Galaxies and Quasars Observed in the *IRAS* Survey (Pasadena: JPL)
Mathewson, D., & Ford, V. 1996, ApJS, 107, 97
Negroponte, J., & White, S. D. 1983, MNRAS, 205, 1009
Osterbrock, D., & Martel, A. 1994, PASP, 104, 76
Rodrigues, I., Dottori, H., Brinks, E., & Mirabel, I. F. 2000, ApJ, 117, 2695
Satoh, C. 1980, PASJ, 32, 41
Sérsic, J. 1968, Atlas de Galaxias Australes (Córdoba: National Univ. Córdoba)
———. 1982, Extragalactic Astronomy (Dordrecht: Reidel)
Soifer, B., Sanders, D., Madore, B., Neugebauer, G., Danielson, G., Elias, J., Lonsdale, C., & Rice, W. 1987, ApJ, 320, 238
Stone, J., & Baldwin, J. 1983, MNRAS, 204, 347
Toomre, A., & Toomre, J. 1972, ApJ, 178, 623
Tully, R. 1988, Nearby Galaxies Catalog (Cambridge: Cambridge Univ. Press)
Veilleux, S., & Osterbrock, D. 1987, ApJS, 63, 295
Young, J., Xie, S., Kenney, J., & Rice, W. 1993, ApJS, 70, 699